# A Millimeter-Wave Micromachined Air-Filled Slot Antenna Fed by Patch

Peiqin Liu, *Student Member, IEEE*, Le Chang, *Student Member*, Yue Li, *Senior Member, IEEE*, Zhijun Zhang, *Fellow, IEEE*, Shaodong Wang, and Zhenghe Feng, *Fellow, IEEE*

***Abstract*— In this paper, a millimeter-wave air-filled slot antenna is presented based on bulk silicon microelectromechanical systems micromachining technology. The antenna is suitable for system-in-package application by utilizing this silicon micromachining technique. To achieve high radiation efficiency in millimeter-wave band, three gold-plated silicon layers are bonded together to realize an air-filled slot antenna. The air-filled structure has the advantages of reducing transmission loss and enhancing the radiation gain. To mitigate the discontinuity between silicon and air, the proposed antenna employs a patch to feed the air-filled structure that also broadens the impedance bandwidth. Owing to the micromachining technique and the air-filled structure, the antenna can be easily integrated with integrated circuit without suffering from dielectric loss. The measured impedance bandwidth of the proposed antenna is 56.3–63.4 GHz, and the measured peak gain is 7.8 dBi at 60 GHz.**

***Index Terms*— Air-filled slot antenna, bulk silicon microelectromechanical systems (MEMS) micromachining technology, millimeter-wave, patch feeding structure.**

## I. Introduction

MILLIMETER-WAVE at 60 GHz has attracted more and more attention in modern short-range communication systems because of the merits of high atmospheric absorption, short wavelength, and wide band [1]. The wavelength at 60 GHz is 5 mm, so it requires high precision for antenna fabrication. Moreover, as operating frequency increases, the dielectric loss tangent increases [2], and the antenna performance suffers from dielectric in millimeter-wave band. Therefore, several technologies are proposed to design millimeter-wave antenna with low-cost, high-efficiency, and easy integration characteristic.

As printed circuit board (PCB) technique has the advantages of low profile, compact size, and easy for fabrication, it is a widely used process technology to design millimeter-wave antennas [3]–[6]. In [3] and [4], substrate integrated waveguide-fed cavity antennas are reported. By incorporating multimode of the cavity, these antennas achieve relative broad bandwidth and even circular polarizations. In [5], a bow-tie antenna with PCB technique is reported to design endfire high-gain antenna. In [6], a planar printed antenna array is proposed to achieve unidirectional radiating characteristic.

Compared to PCB technique, SU-8 film is an attractive choice in millimeter-wave and terahertz applications owing to its ability to form thick and high-resolution structures [7]. An SU-8-based slotted waveguide antenna is proposed in the band of 300 GHz to achieve directional and low-profile properties [8]. Moreover, the SU-8 photoresist is also used to create hollow horn antenna in the millimeter-wave band [9].

Low temperature co-fired ceramic (LTCC) is another excellent candidate to design millimeter-wave antenna [10]. Compared to the PCB technique, LTCC technique is more suitable in the realization of multilayer package-level planar integration at millimeter-wave band [11]. Based on LTCC technique, different kinds of antennas are reported, such as patch antenna [12] and metamaterial-mushroom antenna array [13], and the multilayered LTCC technique can also be utilized in antenna-in-package application [14].

Recently, some millimeter-wave antennas are reported by utilizing micromachined technology [15], [16]. The technique selectively removes substrate portions and bonds different layers together with high precision, which makes it easier to achieve on-chip applications and meet both process reliability specifications and radiation performance [17].

However, the above-mentioned antennas transmit energy through dielectric materials. In the millimeter-waveband, dielectric loss is considerable and it deteriorates antenna efficiency. To solve the problematic issue, some antennas are reported to add air layer to reduce dielectric loss [18]–[22]. In [18], an LTCC corrugated horn antenna is proposed with hollow structure to reduce dielectric loss. In [19], open air cavities are introduced in the LTCC patch antenna array to reduce the losses caused by surface wave and dielectric loss. In [20] and [21], an additional air layer is introduced to form an air-filled waveguide that effectively enhances the antenna efficiency. As the mainstream process technology for multilayer substrates integrated technology, LTCC has the advantages of mechanical stability, thermal conductivity coefficient, and enabling easy 3-D integration [12]. However, LTCC is based on ceramic fabrication instead of the silicon process technology, so it is more complicated to integrate the

Manuscript received December 17, 2016; revised March 7, 2017 and April 24, 2017; accepted May 29, 2017. Date of publication June 26, 2017; date of current version October 5, 2017. This work was supported in part by the National Basic Research Program of China under contract 2013CB329002, and in part by the National Natural Science Foundation of China under contract 61525104. Recommended for publication by Associate Editor E.-X. Liu upon evaluation of reviewers' comments. *(Corresponding author: Zhijun Zhang.)*

P. Liu, L. Chang, Y. Li, Z. Zhang, and Z. Feng are with the State Key Laboratory on Microwave and Communications, Tsinghua National Laboratory for Information Science and Technology, Tsinghua University, Beijing 100084, China (e-mail: zjzh@tsinghua.edu.cn).

S. Wang is with Hebei Semiconductor Research Institute, Shijiazhuang 050000, China.

Color versions of one or more of the figures in this paper are available online at http://ieeexplore.ieee.org.

Digital Object Identifier 10.1109/TCPMT.2017.2711361

integrated circuits (ICs) with the LTCC antennas. Recently, the bulk silicon microelectromechanical systems (MEMSs) technology is utilized to design millimeter-wave antenna [22], [23]. In [22], a leaky-wave antenna is proposed based on the MEMS micromachining technology. However, this antenna is fed by waveguide, and it is not suitable to integrate with chip. In [23], a simulated antenna model is proposed to excite an air-filled slot antenna. However, further measured results show the antenna suffers from gain deterioration problem due to fabrication tolerance.

In this paper, bulk silicon MEMS technology is utilized to realize a millimeter-wave air-filled slot antenna. By adopting this MEMS technology, the antenna can be fabricated with silicon wafer, which means it can be integrated with conventional IC easily and it is beneficial to achieve monolithic integration RF system. The proposed antenna is composed of an air-filled cavity and two air-filled radiation slots to reduce dielectric loss and increase radiation efficiency. Due to the permittivity difference between silicon ($\varepsilon_r = 11.9$) and air ($\varepsilon_r = 1$), there are some challenges in feeding an air-filled resonant cavity. To solve the problem, a patch is introduced to excite the air-filled antenna, and it also broadens the impedance bandwidth. In practical application, the proposed antenna is fed by a ground-signal-ground (GSG) feeding structure that makes it suitable for the system-in-package (SiP) application. However, owing to the limitation of radiation pattern measurement, an antenna with waveguide feeding structure is also fabricated to verify the radiation property. The measured impedance bandwidth of the proposed antenna is 56.3–63.4 GHz, and the measured peak gain is 7.8 dBi at 60 GHz.

## II. Antenna Design

### A. Configuration

Fig. 1 illustrates the topology of the proposed antenna, which consists of three micromachined silicon substrate ($\varepsilon_r = 11.9$) layers. The thickness of each silicon plate is 0.4 mm. The thickness determines the dimension of the resonators in the proposed antenna. Hence, the substrate thickness has effect on the Q-factor and bandwidth of the proposed antenna. As shown in Fig. 1(b), the first layer has two air-filled slots working as the radiation aperture, and every face of the first layer is gold-plated. Fig. 1(c) and (d) depicts the front view and back view of the second layer. The second layer is gold-plated only in top face and bottom face, and the silicon is exposed in other faces. In the second layer, vias are used to form the air-filled resonant cavity. The proposed antenna uses vias instead of gold plating to form the air-filled resonator because the gold-plating process cannot plate the side faces of the air resonator while simultaneously leaving the side faces of the silicon patch exposed. Thus, the proposed antenna utilizes the vias to from the electric wall of the resonator. At the left side of the second layer, a GSG feeding structure is etched to excite the antenna. As shown in Fig. 1(e), the third layer is a whole silicon substrate without penetration etching, and every side of the third layer is gold-plated. Finally, the three layers are bonded together by the wafer direct bonding technology. It is necessary to mention that the first and third layers use silicon substrate instead of metal plate, so the three substrate layers have uniform thermal expansion coefficient, which is beneficial for practical applications.

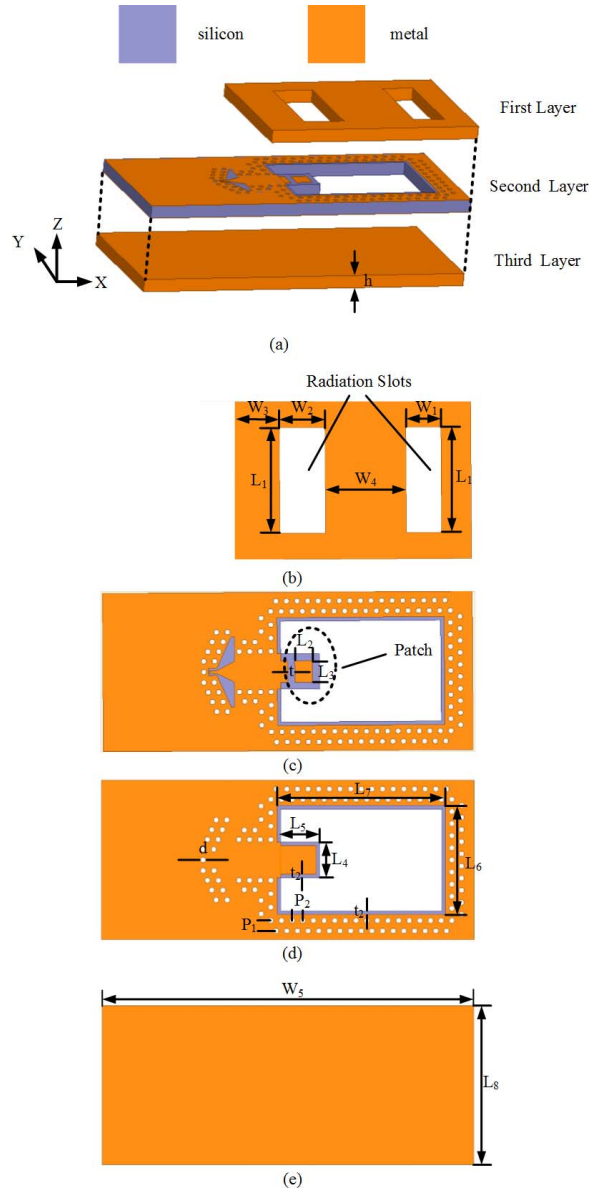


Fig. 1. (a) Proposed antenna array using GSG feeding structure. (b) Top view of the first layer. (c) Top view of the second layer. (d) Bottom view of the second layer. (e) Top view of the third layer.

TABLE I
Dimensions of the Proposed Antenna (Unit: mm)

| $L_1$ | $L_2$ | $L_3$ | $L_4$ | $L_5$ | $L_6$ | $L_7$ |
|---|---|---|---|---|---|---|
| 3 | 0.5 | 0.6 | 1 | 1.1 | 3.07 | 4.75 |
| $L_8$ | $W_1$ | $W_2$ | $W_3$ | $W_4$ | $W_5$ | t |
| 4.5 | 1 | 1.3 | 1.3 | 2.3 | 10.5 | 0.2 |
| $t_2$ | d | $P_1$ | $P_2$ | h | | |
| 0.1 | 0.15 | 0.29 | 0.3 | 0.4 | | |

The parameters of the proposed antenna are optimized by ANSYS High-Frequency Structure Simulator (HFSS) version 14. The optimized values are listed in Table I.

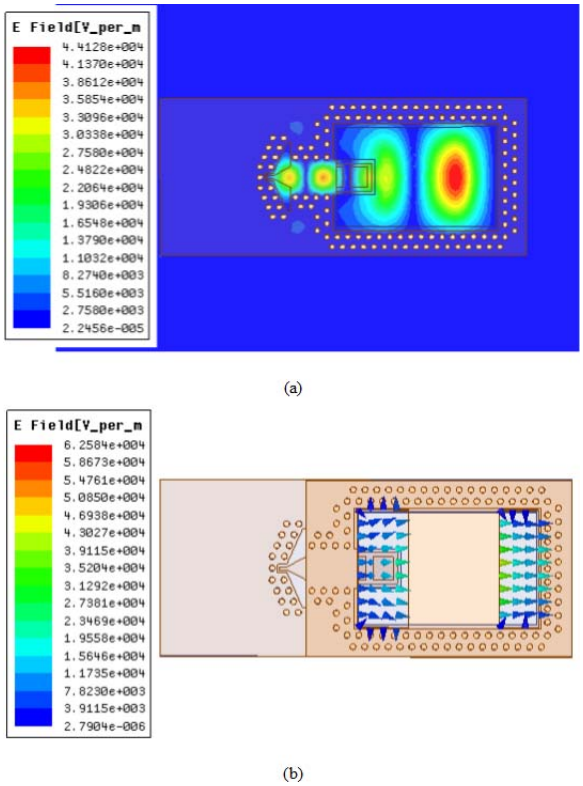


Fig. 2. Electric field distributions of the proposed antenna at 60 GHz. (a) Magnitude electric field distribution inside the second layer. (b) Vector electric field distribution at the radiation aperture of slots.

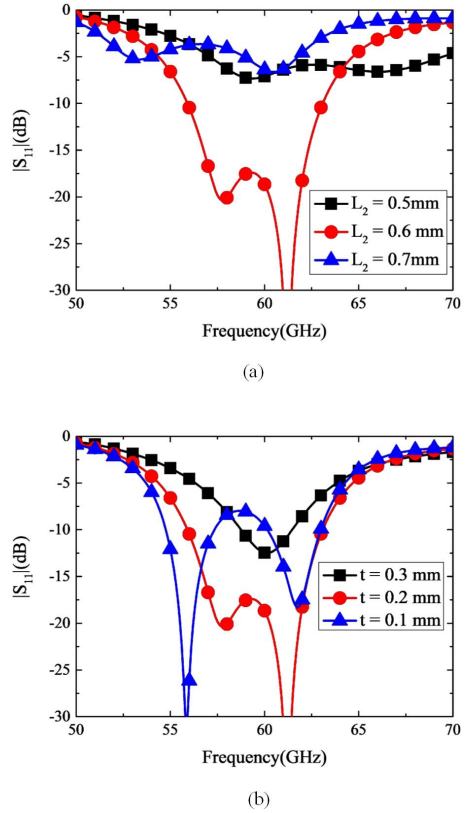


Fig. 3. Simulated $|S_{11}|$ response with different value of the patch feeding structure. (a) $L_2$. (b) $t$.

### *B. Function of the Patch*

For the proposed antenna, the air-filled resonant cavity and slots are utilized to mitigate the dielectric loss. However, the permittivity of silicon is 11.9, which is much larger than the permittivity of air. Thus, it is a challenge to excite the air-filled resonator due to the discontinuity between silicon and air. In this paper, a patch is inserted between the silicon waveguide and air-filled resonator to solve the mismatch issue. As shown in Fig. 1(c) and (d), the patch intrudes into the air-filled resonant cavity. The length along $x$-axis of the patch is 0.5 mm, which is about half-wavelength in the silicon ($\varepsilon_r = 11.9$). When the patch resonates, it transfers electromagnetic energy from the silicon waveguide into the air-filled resonator. To validate the function of the patch, the electric field distribution of the proposed antenna at 60 GHz is depicted as shown in Fig. 2. The magnitude of electric field inside the second layer is illustrated in Fig. 2(a), which proves that the $TE_{102}$ mode in the air-filled resonator is successfully excited by the patch feeding structure. Fig. 2(b) is the vector of electric field at the aperture of the radiation slots. From Fig. 2(b), we can observe that the two slots are excited with half-wavelength mode.

### *C. Parametric Study and Discussion*

In the aforementioned HFSS model, the resonator uses vias to form an electric wall and it will consume a lot of time in tuning the parameters. Therefore, we propose a simplified model, which uses perfect electric conductor instead of vias, for the parametric study. For simplicity, the simplified model is not presented here.

For the proposed antenna, it uses the air-filled resonator to couple electromagnetic energy into the radiation slots, so the resonator needs to resonate at the desired frequency of 60 GHz and its dimension is determined first. The other parameters are studied while keeping the dimension of the resonator constant. Figs. 3 and 4 illustrate the parameter study of the proposed antenna. Fig. 3 shows that tuning the dimensions of the patch has a great impact on the impedance match. As shown in Fig. 3(a), when the length of $L_2$ increases from 0.5 to 0.6 mm, one resonant frequency shifts from about 66 to 53 GHz and another resonant frequency only shifts slightly around 60 GHz. This phenomenon indicates the patch structure introduces a resonant frequency and broadens the bandwidth. As shown in Fig. 1(c), parameter $t$ represents the length of the gap between the patch and the silicon waveguide. When the value of $t$ varies, the electromagnetic coupling between silicon waveguide and the patch varies as well. Thus, Fig. 3(b) indicates that the optimized value of $t$ is 0.2 mm, and when it becomes 0.1 or 0.3 mm, the impedance bandwidth will deteriorate.

Fig. 4(a) shows as the length of $L_1$ increases from 2 to 3 mm, one resonant frequency shifts from about 65 to 58 GHz. If $L_1$ becomes longer, the slots in the first layer will be shorted by the gold-plated surface of the second layer. Hence, there is a smaller resonant frequency shift from 58 to 57 GHz when $L_1$ increases from 3 to 3.5 mm. Besides this resonant frequency, another resonant frequency only shifts slightly around 60 GHz. Once again, this

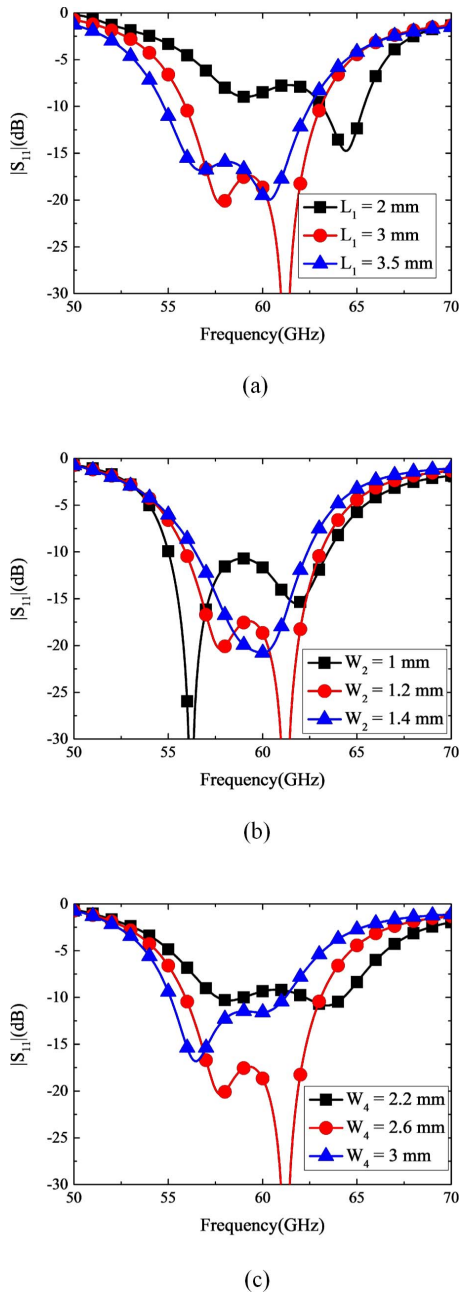


Fig. 4. Simulated $S_{11}$ response with different value of the radiation slot. (a) $L_1$. (b) $W_2$. (c) $W_4$.

phenomenon indicates each slot and patch introduces a resonant frequency, respectively. Fig. 4(b) shows that the variation of the slot's width also has effect on the bandwidth. The reason for the effect is that the width of the slot impacts the electromagnetic coupling between the patch and the air-filled resonator. Fig. 4(c) depicts the distance between the two slots has effect on the impedance match as well. The reason for the phenomenon is that the location of slot has effect on the air-filled resonant cavity, which impacts the impedance.

## III. Fabrication and Measurement

### A. Fabrication

The proposed antenna is fabricated with the bulk silicon MEMS micromachining technology. This technique utilizes

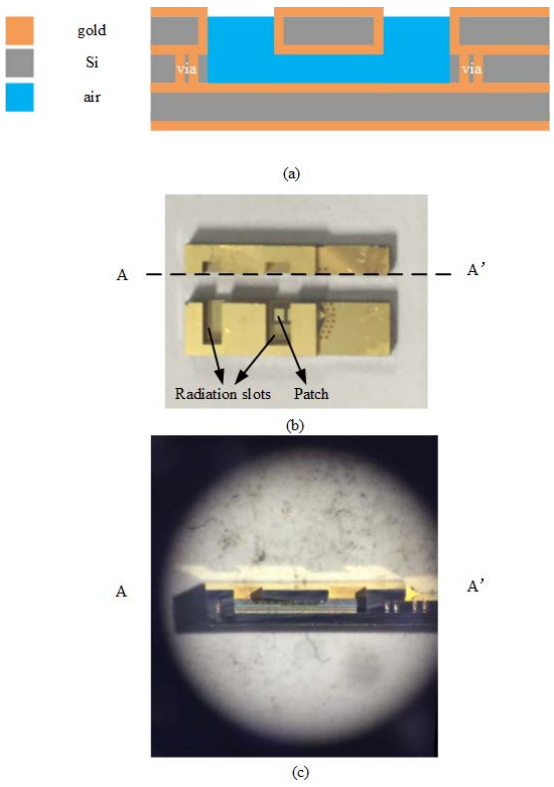


Fig. 5. Description of the multilayer stackup structure. (a) Cross-sectional topology of the micromachined antenna. (b) Photograph of the proposed antenna. (c) Cross-sectional photograph of the proposed antenna.

high-resistivity silicon ($\varepsilon_r = 11.9$) as substrate. The high-resistivity silicon has high electrical resistivity (more than 2000 $\Omega \cdot$ cm), which can reduce the transmission loss [24]. In practice, the high-resistivity silicon in the first layer and the third layer can be replaced by low resistivity. However, in the second layer, it is necessary to use high-resistivity silicon for low-loss transition structure. The low-resistivity ICs can use flip bonding technology to integrate with the proposed antenna.

In order to fabricate the proposed antenna, several processes are utilized. At first, the silicon wafer is penetrated by dry silicon on glass process technology, which uses sulfur hexafluoride gas to etch the single-crystal silicon wafer [24]. The precision of the etching process is $\pm 4$ $\mu$m. Second, the surfaces of the wafers are plated with gold whose thickness is 3.5 $\mu$m. Finally, the wafers are bonded together by using direct bonding technology. The direct bonding technology is based on interatomic interactions without any additional intermediate layer.

Fig. 5 illustrates the fabricating technology of the proposed micromachining antenna. Fig. 5(a) depicts the cross-sectional topology of the proposed antenna. Fig. 5(b) and (c) shows the photograph of the cross section. In this antenna, three silicon wafers are utilized, and the thickness of each wafer is 0.4 mm.

### B. Measurement

As shown in Fig. 5(b), the proposed antenna is fed through a GSG transmission line. The microwave probe positioner is utilized to excite the antenna.

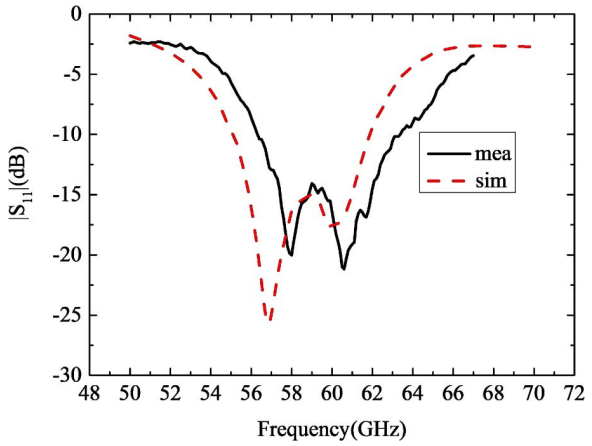


Fig. 6. Simulated and measured reflection coefficients of the proposed antenna fed by GSG.

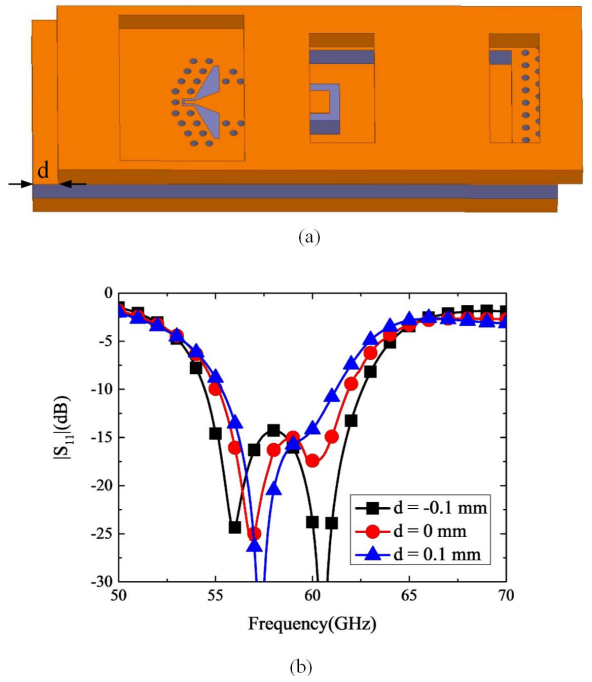


Fig. 7. Study of the layer-to-layer alignment tolerance. (a) Simulated model for studying the alignment tolerance. (b) $|S_{11}|$ responses with different values of $d$.

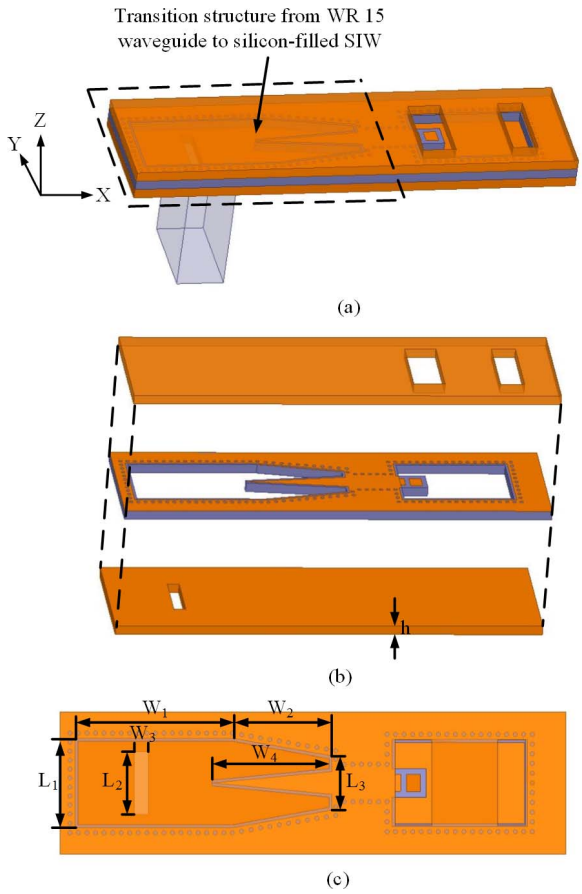


Fig. 8. Geometry of the proposed antenna with waveguide (WR-15) feeding structure. (a) Perspective view. (b) Expanded view. (c) Front view.

TABLE II
DIMENSIONS OF THE PROPOSED ANTENNA (UNIT: mm)

| Parameter | $L_1$ | $L_2$ | $L_3$ | $W_1$ |
|---|---|---|---|---|
| Value | 3.15 | 2.2 | 1.9 | 5.53 |
| Parameter | $W_2$ | $W_3$ | $W_4$ | h |
| Value | 0.62 | 0.5 | 4.1 | 0.4 |

Fig. 6 illustrates the simulated and measured reflection coefficients of the proposed antenna fed by GSG transition structure. The measured −10-dB impedance bandwidth is 56.3–63.4 GHz, which is slightly higher than the simulated results. To analyze the discrepancy between the simulation and measurement, the influence of the layer-to-layer alignment tolerance is studied as shown in Fig. 7. The parameter, in Fig. 7(a), represents the alignment tolerance between the first layer and the second layer. Fig. 7(b) illustrates that the alignment tolerance has effect on $|S_{11}|$ response. Based on these analyses, we can deduce that the discrepancy between simulated and measured results is caused by the alignment tolerance between the silicon substrates.

When it comes to the radiation pattern measurement, the probe positioner obstructs the measurement and we cannot measure the radiation characteristic. To solve the problem, an antenna using waveguide (WR-15) feeding structure is also proposed, fabricated, and measured. The topology of the WR-15 waveguide feeding antenna is illustrated in Fig. 8. The feeding structure adopts a wedge-shaped transition structure [25], whose detailed dimensions are listed in Table II, to transform air-filled waveguide into silicon-filled waveguide. The other part of the antenna is the same as the antenna fed by GSG structure. It should be explained that the antenna fed by WR-15 waveguide is a compromise for radiation measurement and it is not suitable for integration. In the practical application, the GSG feeding antenna is utilized to integrate with ICs and achieve SiP applications.

Fig. 9 shows the photographs of the proposed antenna, which is used in radiation measurement. Fig. 9(a) shows the front view and back view of the antenna. The dimension of the WR-15 feeding antenna is $33 \times 25 \times 1.2$ mm$^3$. The dimension

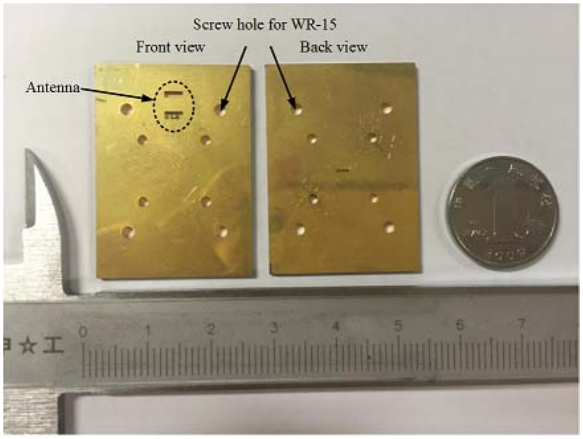


Fig. 9. Photographs of the proposed antennas. (a) Front view and back view of the waveguide feeding antenna. (b) Proposed antenna with WR-15 waveguide.

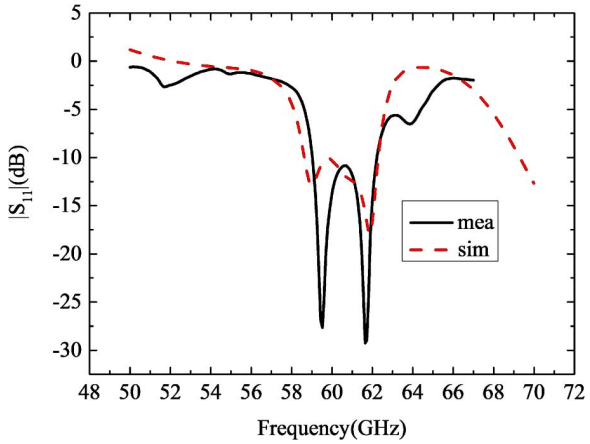


Fig. 10. Simulated and measured reflection coefficients of the antenna fed by WR-15 waveguide.

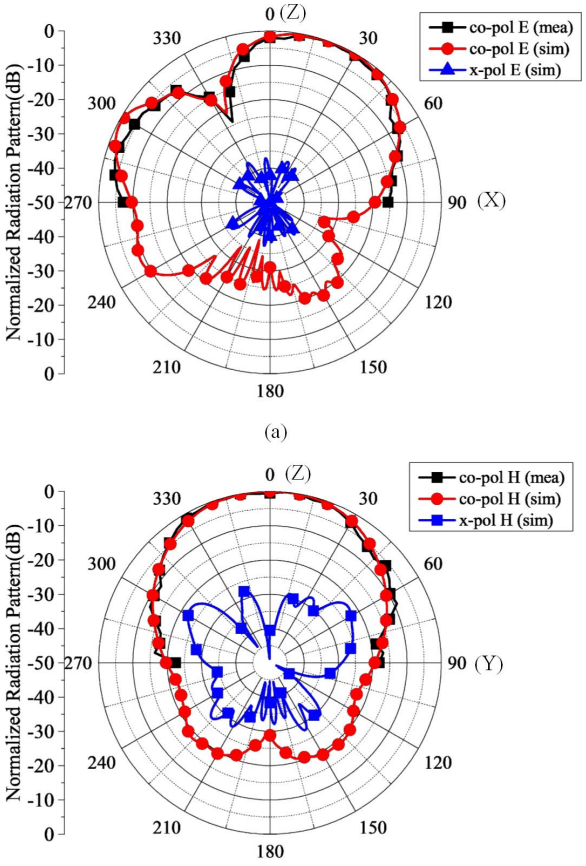


Fig. 11. Normalized radiation patterns of the proposed antenna at 60 GHz. (a) $E$-plane pattern. (b) $H$-plane pattern.

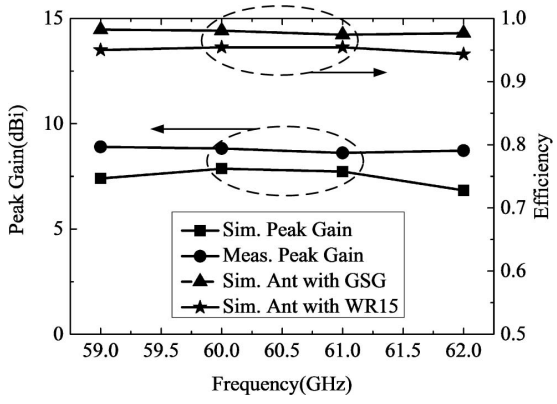


Fig. 12. Peak gain and radiation efficiency of the proposed antenna.

of the GSG feeding antenna is $10.5 \times 4.5 \times 1.2$ mm$^3$ as shown in Fig. 5(b). Fig. 9(b) illustrates the photograph of the proposed antenna with WR-15 waveguide.

Fig. 10 compares the simulated and measured reflection coefficients of the antenna fed by WR-15 waveguide. The measured $-10$-dB impedance bandwidth is 59–62.2 GHz, which agrees well with the simulated result.

Fig. 11 shows the normalized radiation patterns of the proposed antenna fed by WR-15 waveguide at 60 GHz. Simulated and measured normalized $E$-plane patterns are shown in Fig. 11(a). The simulated and measured normalized $H$-plane patterns are shown in Fig. 11(b). In each plane, good agreement between measured and simulated copolarization is achieved. The simulated cross-polarization levels are lower than $-35$ and $-20$ dB for the $E$-plane and $H$-plane, respectively. Due to the measurement limitation, the measured cross-polarization levels are not presented. It can be observed that in the $E$-plane pattern, the pattern is asymmetric and tilts toward $x$-axis. This phenomenon is caused by the patch. Besides the slots, the patch also resonates at the

operating frequency. The resonance of patch has effect on the phase of the left slot and results in the asymmetric pattern. In the millimeter-wave band, the purpose of the antennas in short-range communication system is to radiate effectively. Therefore, the asymmetric pattern is acceptable.

As shown in Fig. 12, the simulated and measured peak gains of the proposed antenna are illustrated. The measured peak gain at 60 GHz is 7.8 dBi, and it is 0.9-dB-less than the simulation. The discrepancy is caused by the alignment and measurement tolerance. Fig. 12 also depicts the simulated radiation efficiency of the proposed antenna with both GSG transition structure and WR-15 feeding structure. The radiation efficiency is about 0.95 over the whole operating band, and it validates that the proposed antenna has high efficiency. The efficiency of WR-15 feeding antenna is slightly lower than that of the GSG feeding antenna because the WR-15 transition structure has more insertion loss than the GSG structure.

## IV. Conclusion

In this paper, bulk silicon MEMS technology is utilized to design millimeter-wave antenna. An air-filled slot antenna is proposed based on the micromachining technology. The antenna consists of three silicon substrates. By the processes of penetration etching, gold plating, and wafer direct bonding, the antenna is achieved with air-filled structure. The air-filled resonator cavity and slots are utilized to reduce dielectric loss and increase radiation efficiency. A patch structure is employed to solve the mismatch issue between silicon and air. Besides the match function, the patch also broadens impedance bandwidth. The measurement results agree well with simulation and validate that the proposed bulk silicon MEMS micromachining antenna has potential for SiP application.

## References


[1] P. Smulders, "Exploiting the 60 GHz band for local wireless multimedia access: Prospects and future directions," *IEEE Commun. Mag.*, vol. 40, no. 1, pp. 140–147, Jan. 2002.

[2] X. C. Zhu *et al.*, "Extraction of dielectric and rough conductor loss of printed circuit board using differential method at microwave frequencies," *IEEE Trans. Microw. Theory Techn.*, vol. 63, no. 2, pp. 494–503, Feb. 2015.

[3] W. Han, F. Yang, J. Ouyan, and P. Yang, "Low-cost wideband and high-gain slotted cavity antenna using high-order modes for millimeter-wave application," *IEEE Trans. Antennas Propag.*, vol. 63, no. 11, pp. 4624–4631, Nov. 2015.

[4] T. Y. Yang, W. Hong, and Y. Zhang, "Wideband millimeter-wave substrate integrated waveguide cavity-backed rectangular patch antenna," *IEEE Antenna Wireless Propag. Lett.*, vol. 13, pp. 205–209, 2014.

[5] A. Dadgarpour, B. Zarghooni, B. S. Virdee, and T. A. Denidni, "Millimeter-wave high-gain SIW end-fire bow-tie antenna," *IEEE Trans. Antennas Propag.*, vol. 63, no. 5, pp. 2337–2342, May 2015.

[6] M. Li and K.-M. Luk, "A low-profile unidirectional printed antenna for millimeter-wave applications," *IEEE Trans. Antennas Propag.*, vol. 62, no. 3, pp. 1232–1237, Mar. 2014.

[7] N. Ghalichechian and K. Sertel, "Permittivity and loss characterization of SU-8 films for mmW and terahertz applications," *IEEE Antennas Wireless Propag. Lett.*, vol. 14, pp. 723–726, 2015.

[8] Y. Wang, M. Ke, M. J. Lancaster, and J. Chen, "Micromachined 300-GHz SU-8-based slotted waveguide antenna," *IEEE Antennas Wireless Propag. Lett.*, vol. 10, pp. 573–576, 2011.

[9] N. A. Murad, M. J. Lancaster, P. Gardner, M. L. Ke, and Y. Wang, "Micromachined H-plane horn antenna manufactured using thick SU-8 photoresist," *Electron. Lett.*, vol. 46, pp. 743–745, May 2010.

[10] Y. Li, Z. N. Chen, X. Qing, Z. Zhang, J. Xu, and Z. Feng, "Axial ratio bandwidth enhancement of 60 GHz substrate integrated waveguide-fed circularly polarized LTCC antenna array," *IEEE Antenna Propag.*, vol. 60, no. 10, pp. 4619–4626, Oct. 2012.

[11] J. Xu, Z. N. Chen, and X. Qing, "270-GHz LTCC-integrated high gain cavity-backed Fresnel zone plate lens antenna," *IEEE Trans. Antennas Propag.*, vol. 61, no. 4, pp. 1679–1687, Apr. 2013.

[12] X. Wang and A. Stelzer, "A 79-GHz LTCC patch array antenna using a laminated waveguide-based vertical parallel feed," *IEEE Antennas Wireless Propag. Lett.*, vol. 12, pp. 987–990, 2013.

[13] W. Liu, Z. N. Chen, and X. Qing, "60-GHz thin broadband high-gain LTCC metamaterial-mushroom antenna array," *IEEE Trans. Antennas Propag.*, vol. 62, no. 9, pp. 4592–4601, Sep. 2014.

[14] B. Cao, H. Wang, Y. Huang, J. Wang, and H. Xu, "A novel antenna-in-package with LTCC technology for W-band application," *IEEE Antennas Wireless Propag. Lett.*, vol. 13, pp. 357–360, 2014.

[15] H. Mopidevi *et al.*, "Three-dimensional microfabricated broadband patch antenna for WiGig applications," *IEEE Antennas Wireless Propag. Lett.*, vol. 13, pp. 828–831, 2014.

[16] W. T. Khan, A. C. Ulusoy, G. Dufour, M. Kaynak, B. Tillack, and J. D. Cressler, "A D-band micromachined end-fire antenna in 130-nm SiGeBiCMOS technology," *IEEE Trans. Antennas Propag.*, vol. 63, no. 6, pp. 2449–2459, Jun. 2015.

[17] N. Jastram and D. S. Filipovic, "Design of a wideband millimeter wave micromachined Rotman lens," *IEEE Trans. Antennas Propag.*, vol. 63, no. 6, pp. 2790–2796, Jun. 2015.

[18] T. Tajima, H.-J. Song, K. Ajito, M. Yaita, and N. Kukutsu, "300-GHz step-profiled corrugated horn antenna integrated in LTCC," *IEEE Trans. Antennas Propag.*, vol. 62, no. 11, pp. 5437–5444, Nov. 2014.

[19] S. B. Yeap, Z. N. Chen, and X. Qing, "Gain-enhanced 60-GHz LTCC antenna array with open air cavities," *IEEE Trans. Antennas Propag.*, vol. 59, no. 9, pp. 3470–3473, Sep. 2011.

[20] Y. She, R. Fujino, J. Hirokawa, M. Ando, D. Hanatani, and M. Fujimoto, "LTCC oversized rectangular waveguide slot array antenna with air-layer in the radiating part in the millimeter-wave band," *IEEE Trans. Antennas Propag.*, vol. 61, no. 4, pp. 1777–1783, Apr. 2013.

[21] Y. She, J. Hirokawa, M. Ando, D. Hanatani, and M. Fujimoto, "LTCC oversized rectangular waveguide slot array antenna with air layers," *IEEE Trans. Antennas Propag.*, vol. 63, no. 12, pp. 5850–5854, Dec. 2015.

[22] L. Chang, Z. Zhang, Y. Li, S. Wang, and Z. Feng, "60-GHz air substrate leaky-wave antenna based on MEMS micromachining technology," *IEEE Trans. Compon., Packag., Manuf. Technol.*, vol. 6, no. 11, pp. 1656–1662, Nov. 2016.

[23] S. Wang, P. Liu, and Z. Zhang, "A 60 GHz slot antenna based on MEMS bulk micromaching technology," in *Proc. IEEE MTT-S Int. Microw. Workshop Ser. Adv. Mater. Process. RF THz Appl. (IMWS-AMP)*, 2016, pp. 1–3.

[24] S. B. Evseev, L. K. Nanver, and S. Milosaviljevic, "Surface-charge-layer sheet-resistance measurements for evaluating interface RF losses on high-resistivity-silicon substrates," *IEEE Trans. Microw. Theory Techn.*, vol. 60, no. 11, pp. 3542–3550, Nov. 2012.

[25] D. Dousset, K. Wu, and S. Claude, "Millimetre-wave broadband transition of substrate-integrated waveguide to rectangular waveguide," *Electron. Lett.*, vol. 46, no. 24, pp. 1610–1611, Nov. 2010.


**Peiqin Liu** (S'17) received the B.S. degree from the University of Electronic Science and Technology of China, Chengdu, China, in 2014. He is currently pursuing the Ph.D. degree in electrical engineering with Tsinghua University, Beijing, China.

His current research interests include antenna design and theory, particularly in antenna arrays based on leaky-wave antenna, massive multiple-input–multiple-output antenna array, and millimeter-wave antenna array.

**Le Chang** (S'16) received the B.S. degree in electronics and information engineering from Xidian University, Xi'an, China, in 2012. He is currently pursuing the Ph.D. degree in electrical engineering with Tsinghua University, Beijing, China.

His current research interests include antenna design and theory, particularly in antenna arrays based on transmission lines, transmitted arrays, leaky-wave antennas, and millimeter-wave and terahertz antennas based on silicon micromachining technology.

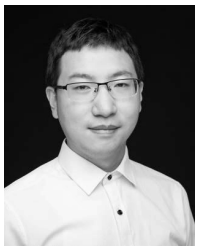

**Yue Li** (S'11–M'12–SM'17) received the B.S. degree in telecommunication engineering from the Zhejiang University, Zhejiang, China, in 2007, and the Ph.D. degree in electronic engineering from Tsinghua University, Beijing, China, in 2012.

He was a Visiting Scholar with the Institute for Infocomm Research, and with A*STAR, Singapore, in 2010. In 2012, he was a Visiting Scholar with the Hawaii Center of Advanced Communication, University of Hawaii at Manoa, Honolulu, HI, USA, and a Post-Doctoral Fellow with the Department of Electronic Engineering, Tsinghua University. In 2013, he was a Research Scholar with the Department of Electrical and Systems Engineering, University of Pennsylvania, Philadelphia, PA, USA. Since 2016, he has been with Tsinghua University, where he is currently an Assistant Professor with the Department of Electronic Engineering. He has authored or coauthored over 80 journal papers and 30 international conference papers, and holds 15 granted Chinese patents. His current research interests include metamaterials, plasmonics, electromagnetics, nanocircuits, mobile and handset antennas, multiple-input–multiple-output and diversity antennas, and millimeter-wave antennas and arrays.

Dr. Li received the Issac Koga Gold Medal from URSI General Assembly in 2017, the Young Scientist Award from URSI AP-RASC 2016, the Young Scientist Awards from EMTS 2016, the Best Student Paper Award ICMMT 2016, the Best Paper Award from ISAPE 2016, the Young Scientist Awards from URSI General Assembly in 2014, the Outstanding Doctoral Dissertation of Beijing Municipality in 2013, and the Principal Scholarship of Tsinghua University in 2011.

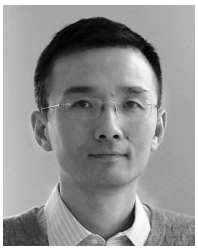

**Zhijun Zhang** (M'00–SM'04–F'15) received the B.S. and M.S. degrees from the University of Electronic Science and Technology of China, Chengdu, China, in 1992 and 1995, respectively, and the Ph.D. degree from Tsinghua University, Beijing, China, in 1999.

In 1999, he was a Post-Doctoral Fellow with the Department of Electrical Engineering, University of Utah, Salt Lake City, UT, USA, where he was appointed as a Research Assistant Professor in 2001. In 2002, he joined the University of Hawaii at Manoa, Honolulu, HI, USA, as an Assistant Researcher, and Amphenol T&M Antennas, Vernon Hills, IL, USA, as a Senior Staff Antenna Development Engineer, and was then promoted as an Antenna Engineer Manager. In 2004, he joined Nokia Inc., San Diego, CA, USA, as a Senior Antenna Design Engineer. In 2006, he joined Apple Inc., Cupertino, CA, USA, as a Senior Antenna Design Engineer and was then promoted to a Principal Antenna Engineer. Since 2007, he has been with Tsinghua University, where he is currently a Professor with the Department of Electronic Engineering. He has authored *Antenna Design for Mobile Devices* (Wiley, 1st ed. 2011, 2nd ed. 2017).

Dr. Zhang served as an Associate Editor of the IEEE TRANSACTIONS ON ANTENNAS AND PROPAGATION from 2010 to 2014 and the IEEE ANTENNAS AND WIRELESS PROPAGATION LETTERS from 2009 to 2015.

**Shaodong Wang,** photograph and biography not available at the time of publication.

**Zhenghe Feng** (M'05–SM'08–F'12) received the B.S. degree in radio and electronics from Tsinghua University, Beijing, China, in 1970.

Since 1970, he has been with Tsinghua University as an Assistant, Lecture, Associate Professor, and Full Professor. His current research interests include numerical techniques and computational electromagnetics, RF and microwave circuits and antenna, wireless communications, smart antenna, and spatial temporal signal processing.